Raspberry Pi-based Motion Control Testbed for Mechatronics Education

Martin Goubej* **Lukáš Bláha***

NTIS Research Centre, Faculty of Applied Sciences,
University of West Bohemia, Pilsen, Czechia,
(e-mail: mgoubej@ntis.zcu.cz),
** (e-mail: frere@ntis.zcu.cz).*

Abstract: The paper deals with the development of an experimental benchmark mechatronic system that was employed in control courses taught at our university. The first part introduces its mechanical design, installed instrumentation and software environment. Methodology of its use in terms of our control courses curriculum follows, highlighting particular problems that students can solve during their classes. The last section summarises our observations regarding the contribution of this tool to the effectiveness of the education process.

Keywords: control education, motion control, mechatronics, hardware-in-the-loop, HIL, two-mass system, Raspberry Pi

1. INTRODUCTION

Motion control systems belong to key enabling technologies in many fields of industrial manufacturing, ranging from robotics through CNC machine tools to semiconductor production and precision engineering. Systematic application of advanced control approaches is a necessary prerequisite for achieving performance limits of new generation machines and production systems (Čech et al., 2021). The ever-increasing demands on precision, speed and adaptability of motion systems imply entirely new demands on control curricula for master degree students (Čech et al., 2019). Therefore, various control-related aspects of mechatronics should become an essential part of the education process ongoing at technical universities.

One of the main observed challenges is to establish a deep understanding of connections between theory and practical implementation of control systems, including all HW and SW related topics (Shiller, 2013). The role of hands-on experience with physical devices remains invaluable and can hardly be fully substituted by offline numerical simulations (Craig, 2001). The most direct way to expose students to control systems technology is to use actual production machines and setups for education. The advantage of the realistic representation of real-world problems comes at the cost of considerable maintenance and purchasing expenses. Safety aspects, limited availability in higher quantities and rapid technology ageing may also be an issue. A compromise is often sought by introducing problem-oriented simplified setups, either in the form of physical models (Reck, 2018), or Hardware-in-the-loop (HIL) simulators (Sobota et al., 2019; Goubej and Langmajer, 2020).

The paper aims to share our experience in designing and employing one such physical setup tailored to meet the requirements of teaching mechatronics in our control courses. Description of HW and SW components and best practices of its use follow in the next sections.

Fig. 1. Motion setup: mechanically coupled 2DoF system

2. MECHANICAL DESIGN

Our main goal was to develop an affordable motion stage fulfilling a few fundamental objectives:

- reasonable purchasing/maintenance costs
- simple modular structure with easy configurability by using 3D-printed components
- close testbed-model conformity
- safety, robustness and easy handling
- wide range of reproducible motion control problems

This has led us to the mechanically compliant 2DoF system shown in Fig. 1. The relevance to practice is given by its dynamic characteristics of two-mass or multi-mass structure that resembles many practical motion systems such as elastic robotic joints, flexible arm manipulators, machine tool feed drives or rolling-mills (Yakub et al., 2012).

The testbed is supported by a solid mounting plate with railways. These railways are used for assembly and configuration adjustments. The moving parts are placed on top of the plate via base pillars. The pillar material (Polylactic acid - PLA) is chosen to be different from the plate to

reduce vibration transmission to the base and the rest of the setup.

The rotor system consists of two servomotors directly connected via a torsional shaft and a flexible coupling. The torsional bar was designed to fulfil specific demands on the resonance behaviour of the system. The flexible coupling is used to eliminate axial misalignment of the connected shafts. This type of connection does not introduce any backlash, which is fundamental for the purposed of high-fidelity motion control. Load inertia can be varied via an additional flywheel directly attached to the motor shaft connection mount, such that the shaft flexibility is not affected.

Mechanical robustness is ensured by using durable and lightweight 20x20mm Item profiles, creating a self supporting construction that is easy to unmount and handle. Safety barriers are made by inserting polycarbonate walls. The total size 40 (L) x 20 (W) x 19 (H) [cm] and weight less than 8kg are kept deep below hygienic portability limits. Also, the required storage space is low.

3. INSTRUMENTATION AND REAL-TIME SOFTWARE ENVIRONMENT

The goal was to avoid development of custom-made electronics and equip the setup with commercially available automation components, to ensure long-term serviceability. The electrical part of the testbed consists of two servo motors with position encoders, corresponding motor controllers, Raspberry Pi single-board computer and Monarco HAT industrial grade I/O board.

Technical details are briefly summarised as follows:

Motors

- Brushless DC motor Nanotec DB43M024030 encapsulated in NEMA 17 housing
- rated speed 3000 rpm, rated torque 17 Ncm, rotor inertia 60 gcm^2
- optical incremental encoder with 20000 CPR resolution

Motor controllers

- 2x Maxon MAXPOS 50/5 motor controller with built in EtherCAT communication
- wide range of operating modes including Cyclic Snchronous Torque loop
- cycle times up to $100\mu s$

Embedded PC

- Raspberry Pi 4 with 64-bit quad-core processor
- @1.5 GHz, up to 8GB LPDDR4, Gigabit Ethernet, USB3.0, Standard 40-pin GPIO header

I/O board

- Monarco HAT I/O board for Raspberry Pi
- mountable on Standard 40-pin GPIO header
- 10-30V DC power supply, analog and digital I/O
- 1-Wire bus, RS-485, RTC chip
- metal enclosure for DIN-rail mounting

The testbed is powered by REXYGEN system, providing a software environment for rapid real-time control
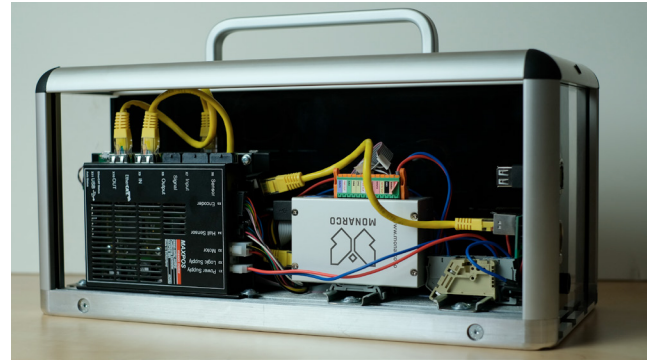

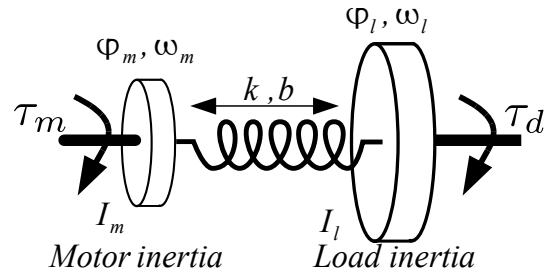Fig. 2. Under the hood: Raspberry Pi+Monarco HAT controller with a pair of servo amplifiers

Fig. 3. Compliant two-mass system representing the dominant resonance mode behaviour

prototyping (REX Controls s.r.o., 2022). The application development is based on graphical programming without hand-coding with a workflow very similar to Matlab-Simulink. Python or C-like scripting and sequential function chart support are also included, allowing the development of complex user applications. The programmed algorithms can optionally be simulated and validated offline in Simulink. However, a Matlab license is not required for real-time control.

4. EMPLOYMENT IN CONTROL CURRICULUM

4.1 Plant modelling and identification

The motion system under study is a mechanical continuum with a theoretically infinite number of bending modes caused by distributed rotor elasticity. However, the testbed construction and dimensioning of the compliant element is made to intentionally introduce only one or two dominant flexible modes at frequencies relevant for motion control (units to dozens of hertz).

For the purpose of modelling, a two-mass system shown in Fig. (3) can be considered as a generic simplified representation of a compliant mechanical load with single dominant resonance mode. The inertia of a driving motor I_m is connected to a load I_L by a flexible shaft modelled as a linear torsional spring described by the stiffness constant k and internal viscous friction coefficient b. The corresponding equations of motion are given as:

$$\varepsilon_m = \dot{\omega}_m = \frac{1}{I_m}\{\tau_m - k(\varphi_m - \varphi_l) - b(\omega_m - \omega_l)\},$$

$$\varepsilon_l = \dot{\omega}_l = \frac{1}{I_l}\{\tau_d + k(\varphi_m - \varphi_l) + b(\omega_m - \omega_l)\}, \quad (1)$$

where φ, ω and ε denote angular position, velocity and acceleration of the inertial loads. The transfer functions from the driving motor torque τ_m to the motor and load velocities are obtained as

$$P_m(s) = \frac{\omega_m(s)}{\tau_m(s)} = \frac{I_l s^2 + bs + k}{s[I_m I_l s^2 + b(I_m + I_l)s + k(I_m + I_l)]} =$$
$$= \frac{K_1}{s} \frac{s^2 + 2\xi_z \omega_z s + \omega_z^2}{s^2 + 2\xi \omega_n s + \omega_n^2},$$
$$P_l(s) = \frac{\omega_l(s)}{\tau_m(s)} = \frac{bs + k}{s[I_m I_l s^2 + b(I_m + I_l)s + k(I_m + I_l)]} =$$
$$= \frac{K_2}{s} \frac{s + \frac{\omega_z}{2\xi_z}}{s^2 + 2\xi \omega_n s + \omega_n^2}, \quad (2)$$

where the corresponding gains, natural frequencies and damping factors can be expressed by means of the plant parameters

$$K_1 = \frac{\omega_n^2}{(I_l + I_m)\omega_z^2}, \ \omega_n = \sqrt{\frac{k(I_l + I_m)}{I_l I_m}}, \ \omega_z = \sqrt{\frac{k}{I_l}},$$
$$K_2 = \frac{2\xi_z \omega_n^2}{(I_l + I_m)\omega_z}, \ \xi = \sqrt{\frac{b^2(I_l + I_m)}{4k I_l I_m}}, \ \xi_z = \sqrt{\frac{b^2}{4k I_l}}. (3)$$

The parameter of so called *resonance ratio* is defined as

$$r = \frac{\omega_n}{\omega_z} = \frac{\xi}{\xi_z} = \sqrt{1 + R}, \ R = \frac{I_l}{I_m}, \quad (4)$$

where R is the *load to drive inertia* ratio.

The resonance ratio parameter is a fundamental quantity determining the achievable performance of the motion system. Goubej (2016) showed that low resonance ratio systems are difficult to control in terms of attaining a sufficient amount of damping, whereas a high resonance ratio tends to cause low closed-loop bandwidth and sluggish response times. Optimal performance is achieved for $r \approx 2$. Students can experience this by experimenting with exchangeable flywheels of different sizes determining the load inertia I_l.

The effects of external disturbances in terms of the load torque τ_d can also be studied by deriving the corresponding transfer functions

$$P_{ld}(s) = \frac{\omega_l(s)}{\tau_d(s)} = \frac{I_m s^2 + bs + k}{s[I_l I_m s^2 + b(I_l + I_m)s + k(I_l + I_m)]},$$
$$P_{md}(s) = \frac{\omega_m}{\tau_d} = P_l(s), \quad (5)$$

revealing a symmetry with (2) due to the structure of the equations of motion in (1).

The overall dynamics can be expressed by means of a 2×2 transfer function matrix

$$\begin{bmatrix} \omega_m(s) \\ \omega_l(s) \end{bmatrix} = \begin{bmatrix} P_m(s) & P_{md}(s) \\ P_l(s) & P_{ld}(s) \end{bmatrix} \begin{bmatrix} \tau_m(s) \\ \tau_d(s) \end{bmatrix} \triangleq P(s) \begin{bmatrix} \tau_m(s) \\ \tau_d(s) \end{bmatrix}. \quad (6)$$

The role of the disturbance torque τ_d that can be directly controlled by the second actuator may differ based on the formulated control scenario. It can serve as an external load-side disturbance acting on a SISO control loop with τ_m assigned as the plant input. Alternatively, both actuators can be used simultaneously, aiming at controlling velocity or position of both sides of the motion stage, forming a multi-variable feedback design problem.
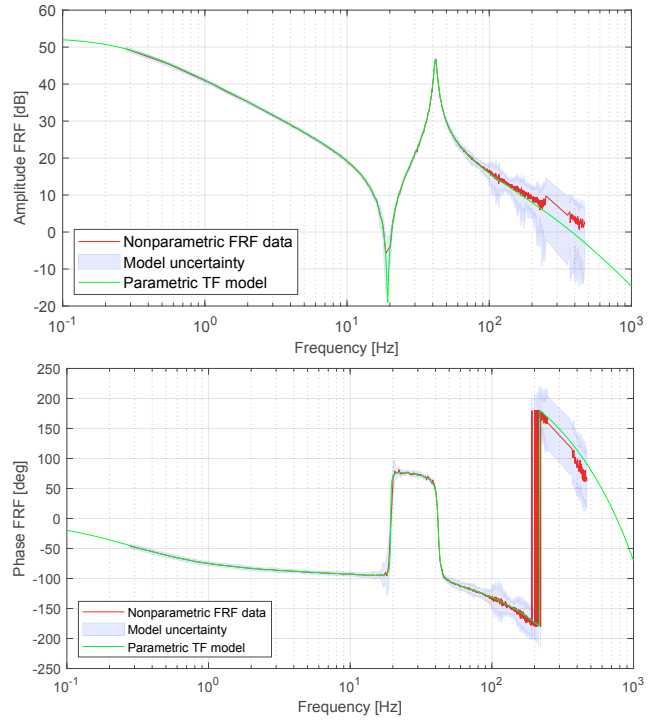

Fig. 4. Experimental identification of motor torque to motor velocity dynamics: red - nonparametric frequency response function model, green - parametric transfer function model, blue - model confidence bounds

The simplified model is used to explain fundamental problems in controlling flexible motion systems. Students are asked to analyse the influence of the parameters on the overall dynamics, allowing them to gain a deeper physical understanding of the system's behaviour. Principles of resonances and anti-resonances are explained and demonstrated in time- and frequency-domain responses. Differences between the rigid and flexible mode of operations are clarified, emphasising the importance of the relative position of the system resonances with respect to the target closed-loop bandwidth.

The analytical two-mass model is a good starting point to gain initial insight into plant dynamics. However, uncertain parameters and unmodelled dynamics due to higher bending modes, friction and actuator lag prevent it from being used directly for control design. Therefore, in the next step, students try to derive a control-relevant model from the experimental data. They are taught how to synthesise proper wide-band excitation signals with favourable properties such as pseudo-random binary sequences or optimal-phase multi-sines. State of the art methods in linear or nonlinear system identification can be demonstrated, ranging from ordinary least squares or instrumental variables through prediction error method, subspace identification to complex transfer function fitting in the frequency domain, both in SISO or MIMO setting, see e.g. Ljung (1999), Pintelon and Schoukens (2012). This forms a baseline for the subsequent steps of model-based control design.

An example of frequency-domain identification is shown in Fig. (4). Time-domain data acquired from an experiment with the motion setup were used to generate non-
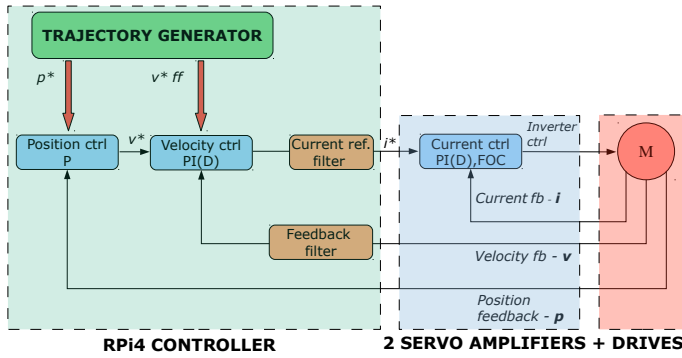
Fig. 5. Cascade PID scheme implementing current, velocity and position control loops

parametric frequency response function (FRF) model. In the next step, linear plant model was fitted to the FRF data using a Maximum-likelihood estimator, resulting in a 4th order plus dead-time transfer function

$$P_m(s) = \frac{\omega_m(s)}{\tau_m(s)} =$$

$$= \underbrace{\left(\frac{K}{\tau_1 s + 1}\right)}_{\text{rigid mode}} \underbrace{\left(\frac{s^2 + 2\xi_z \omega_z s + \omega_z^2}{s^2 + 2\xi \omega_n s + \omega_n^2}\right)}_{\text{flexible mode}} \underbrace{\left(\frac{1}{\tau_2 s + 1}\right)}_{\text{actuator lag}} \underbrace{e^{(-7.5E-4)s}}_{\substack{\text{network} \\ \text{delay}}},$$

$$K = 2047, \ \tau_1 = 0.57s, \ \tau_2 = 0.0012s, \ \xi_{z1} = 0.0099,$$

$$\omega_{z1} = 119 \frac{\text{rad}}{\text{s}}, \xi_1 = 0.02, \ \omega_n = 263 \frac{\text{rad}}{\text{s}}. \tag{7}$$

Proper structure of the parametric model has to be determined prior to optimisation-based fitting to the FRF data. Students are asked to discuss possible choices based on the preliminary physical analysis of the idealised two-mass system and knowledge of the installed instrumentation. The structure in (7) extends the analytical model from (2) by adding viscous friction and a first-order lag to introduce motor current loop dynamics. The last component is a priori known pure time delay caused by the timing of the EtherCAT network connecting the controller HW with the servo amplifiers.

4.2 Active vibration damping via feedback control

Students usually start with the conventional cascade PID control scheme that is prevalent in industrial servo drives (Fig. 5). A low-level current/torque control loop is implemented directly in the servo amplifier, and the main focus is directed towards the velocity and position control loops.

First experiments are usually performed using manual trial-and-error tuning of the velocity controller with the collocated feedback, i.e. using the motor-side velocity ω_m as the plant output. It is demonstrated that the motion stage behaves like an ideal rigid load for sufficiently low gains of a PI(D). The necessity of integral action to achieve zero steady-state error is demonstrated easily by injecting step disturbances using the second actuator. An increase of controller gains to enhance closed-loop bandwidth inevitably leads to transient oscillations at some point. Students realise that fine-tuning the controller by hand gets tricky when the target bandwidth overlaps with the location of the resonance mode of the system. Somewhat counter-intuitive behaviour is observed when

pushing the PID gains as far as possible. While the closed-loop dynamics observed at the motor-side improves, severe oscillations appear at the second actuator designating the manipulated load motion. Physical intuition is developed by explaining that a very stiff motor-side feedback loop creates a new system that behaves like a single mass-spring-damper system connecting the load inertia to the ground via a flexible coupling. This leads to a second-order dynamics with the resonance frequency approaching the antiresonance frequency ω_z of the originally two-mass system in (2), (3).

In the next phase, students are asked to use the plant models acquired from the experimental identification to get accurate predictions concerning closed-loop dynamics and propose a systematic method for the tuning of the PID gains. At first, some classical methods and tuning formulas from the field of electrical drives such as Symmetrical optimum or Optimum modulus are revisited. It is shown that they often fail when considering only the rigid dynamics of the system, ignoring the compliant behaviour of the driven load. Next, a manual loop-shaping design is performed to deliver a set of tuning parameters that achieve robust stability and sufficient damping of all closed-loop modes. The Control system designer application, formerly known as SISOtool in Matlab, proved to be an invaluable didactic tool for this purpose as it allows to combine the loop-shaping with the Evans root-locus method and interactive visualisation of important closed-loop responses. Therefore, the insight acquired from time, frequency and algebraic domains can be combined. The "high-gain paradox" observed during the manual experiments is further explained by examining the root-locus plot. The weakly damped open-loop zeros attract a couple of closed-loop poles. They cancel each other when using sufficiently high controller gain. However, this cancellation occurs only for the motor-side output, whereas the load-side quantities exhibit unwanted oscillations due to the weakly damped closed-loop mode. *The main lesson learned here is that care must be taken when designing feedback loops with different feedback and performance variables*, making it inherently a multivariable control problem.

The manual loop-shaping procedure is then repeated for the non-collocated control setup using the load-side velocity ω_l as feedback output. The students quickly realise that it is much more difficult to properly design the closed-loop controller using the load-side sensing than in the previous case of motor side feedback. Comparison of the two relevant transfer function models P_m, P_l in (2) reveals that the main difficulty comes from the significant phase delay of the latter due to the missing complex zeros.

The role of low-pass current reference and feedback filters in Fig. 5 is also examined thoroughly, emphasising the practical requirement for sufficient high-frequency roll-off in the controller amplitude response. This is learned during hands-on experiments with the setup, as high-gain PIDs without additional filters produce sensible noise due to the amplification of the measurement errors in the feedback signals.

Once the conventional cascade controller works properly, students move to more advanced topics involving:
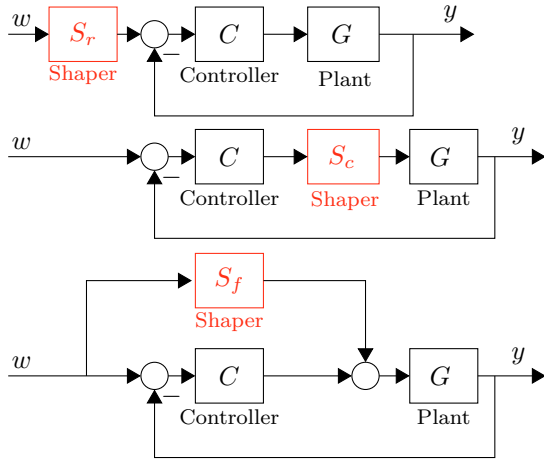
Fig. 6. Application of signal shapers in various control topologies: reference prefiltering (top), control action shaping (centre), feedforward control (bottom)

- Algebraic pole-placement design using state or output feedback
- Observer design (full or reduced order state estimators, Kalman filters, disturbance observers)
- Optimal control using LQR/LQG methodology
- Norm-based control using H_2/H_∞ optimisation
- Robust control
- Multi-variable control

Both state and output feedback-based controllers can be implemented and evaluated thanks to the utilisation of two distinct position/velocity sensors on both sides of the rotor assembly. The dual actuator topology enables reference following as well as active disturbance rejection functionalities to be examined in the SISO setting. Multi-variable (MIMO) control setup is also possible by using both motors as independent inputs, resembling many industrial motion systems with multiple actuators acting on the same degree of freedom, such as turntables or dual-gantry stages. The replaceable parts of the motion stage can be used to emulate changes in the plant dynamics and evaluate robustness to uncertainty. *Students learn that even with sophisticated modern control theory methods, one has to fully understand the design problem* to address all the inherent trade-offs of feedback such as bandwidth vs noise propagation, robust stability concerns, or well-known Bode integral theorems.

4.3 Passive vibration damping using reference/control action shaping and feedforward control

The experiments with various feedback control methods reveal that sufficient amount of closed-loop damping cannot be achieved for certain configurations of the motion setup. Additional control topologies extending the basic 1DoF feedback control loop are introduced aiming at improvement of system's performance (Fig. 6).

Students start with simple notch and biquad filters in the form of

$$S_1(s) = \frac{s^2 + 2\xi\omega_n s + \omega_n^2}{s^2 + 2\omega_n s + \omega_n^2}, S_2(s) = \frac{s^2 + 2\xi\omega_n s + \omega_n^2}{s^2 + 2\xi_z\omega_z s + \omega_z^2} \quad (8)$$

with the parameters chosen to match the poles and/or zeros of the controlled plant dynamics. *Important consequences of the cancellation of weakly damped poles and zeros have to be explained.* For example, by employing one of the shapers from (8) as the control-action filter S_c in Fig. 6, the feedback is effectively disconnected at the resonance frequency, resulting in loss of controllability of the flexible mode. Only passive vibration damping due to reference changes is achieved since any external disturbances still cause an oscillatory response. On the other hand, it is recognised that the feedforward controller S_f essentially needs to realise an inverse of the plant dynamics. Considering the load-side transfer P_l in (2) and a limit zero-damping case $b \to 0$, one needs a non-causal feedforward

$$S_f(s) = \frac{U_f(s)}{W(s)} = c_1 s^4 + c_2 s^2, \quad (9)$$

where U_f denotes the computed feedforward action, W is a position reference and the constants $c_{1,2}$ are to be determined from $S_f = (P_l/s)^{-1}$. Thus, the motion trajectory has to be known in advance and must be smooth up to $4th$ derivative of position (snap) to allow perfect tracking. Discussion on how to synthesise proper motion profiles based on this requirement follows at this point. More advanced shaper types can be introduced later, e.g. the Zero vibration filters in the form of weighted sum of time-delays

$$S_3(s) = \sum_{i=1}^{n} A_i e^{-d_i s}. \quad (10)$$

Proper design of amplitudes A_i and time-delay values d_i allows to derive shapers with favourable properties unattainable with basic filter types in (8), e.g. finite impulse response of flexible modes, explicit robustness to model uncertainty or monotonous output response. Extensive treatment of this topic is given by Singhose (2009), Singh and Vyhlídal (2020) or Goubej et al. (2020).

4.4 Repetitive and iterative learning control

Many practical motion control problems involve exact cancellation of a periodic disturbance or following of a periodic reference trajectory. Our motion stage can be used to emulate both these scenarios due to inherent disturbances arising from the principle of construction:

(1) Torque ripple of the actuators due to electronic commutation and cogging effects
(2) Velocity ripple due to imbalanced load that can be attached to the motor shaft

Both these factors contribute to a clearly periodic motion, observable especially during low-speed operation. Various repetitive control (RC) topologies can be designed and validated, with the goal of tracking error minimisation (Wang et al., 2009).

Iterative learning control (ILC) seeks to optimise the performance of a repeated motion task by recursively adapting a feedforward signal injected in the feedback loop, see Bristow et al. (2006). The main difference to the continuous operation of the RC is that the system state is reset to a defined initial condition after each iteration, and there is a defined finite length of the motion task.

Students start with basic model-free ILC algorithms, such as the PD update law, and continue with more advanced model-based learning algorithms, e.g. frequency-domain or basis-function ILC. It is observed that the performance of the motion system can typically be improved in the order of several magnitudes when compared to purely feedback-based control (Goubej et al., 2019).

5. CONCLUSION

The presented motion testbed proved to be an excellent benchmark system for teaching important topics in mechatronic systems control. It is cheap enough to be purchased for a control lab in higher quantities, simple enough to be well understood by students, but sufficiently complex at the same tame to closely resemble many practical motion control problems. It is currently being used in one undergraduate and one graduate level control courses taught at Department of Cybernetics at University of West Bohemia. We believe that it may be useful also for industry-oriented training and demonstrations. The main benefits for the education process that we perceive can be summarised as follows:

- Much more enthusiasm is observed among students compared to offline numerical simulations
- Hands-on experience with important control design aspects is acquired (unmodelled dynamics, noise, plant nonlinearity, bandwidth limitations) in contrast to ideal simulation environments, where everything usually works as expected
- Maintenance and operational costs as well as potential risks of failures are vastly reduced compared to actual production-level machines and setups, but relevance of the studied problems to practical applications can easily be explained
- Important implementation issues can be taught apart from pure controller design methods, e.g. electrical drives and power electronics, real-time systems and control-oriented programming languages or industrial communications
- The control system development cycle can be demonstrated in all its important stages - from modelling and analysis through simulation, implementation to commissioning and validation

The mechanical and electrical design of the setup was released to public domain. Feel free to contact the authors for more details regarding the testbed specification, sample projects or possible supply of the system as a whole.

ACKNOWLEDGEMENTS

REFERENCES

Bristow, D.A., Tharayil, M., and Alleyne, A.G. (2006). A survey of iterative learning control. *IEEE Control Systems*, 26, 96–114.

Craig, K. (2001). Is anything really new in mechatronics education? *IEEE Robotics and Automation Magazine*, 8(2), 12–19. doi:10.1109/100.932752.

Goubej, M. (2016). Fundamental performance limitations in PID controlled elastic two-mass systems. In *IEEE International Conference on Advanced Intelligent Mechatronics (AIM)*, 828–833. doi: 10.1109/AIM.2016.7576871.

Goubej, M. and Langmajer, M. (2020). Experience with use of HIL simulators in control engineering course. *IFAC-PapersOnLine*, 53(2), 17308–17313. doi: https://doi.org/10.1016/j.ifacol.2020.12.1814.

Goubej, M., Meeusen, S., Mooren, N., and Oomen, T. (2019). Iterative learning control in high-performance motion systems: from theory to implementation. In *2019 24th IEEE International Conference on Emerging Technologies and Factory Automation (ETFA)*. doi: 10.1109/ETFA.2019.8868996.

Goubej, M., Vyhlídal, T., and Schlegel, M. (2020). Frequency weighted H2 optimization of multi-mode input shaper. *Automatica*, 121. doi: https://doi.org/10.1016/j.automatica.2020.109202.

Ljung, L. (1999). *System identification: theory for the user*. Upper Saddle River, NJ, Prentice Hall PTR.

Pintelon, R. and Schoukens, J. (2012). *System Identification: A Frequency Domain Approach*. Wiley-IEEE Press.

Reck, R.M. (2018). Validating DC motor models on the Quanser Qube servo. In *Dynamic Systems and Control Conference*, volume 51906. American Society of Mechanical Engineers.

REX Controls s.r.o. (2022). REXYGEN - Programming automation devices without hand coding. URL http://www.rexygen.com.

Shiller, Z. (2013). A bottom-up approach to teaching robotics and mechatronics to mechanical engineers. *IEEE Transactions on Education*, 56(1), 103–109. doi: 10.1109/TE.2012.2226176.

Singh, T. and Vyhlídal, T. (2020). Recent results in reference prefiltering for precision motion control. *IFAC-PapersOnLine*, 53(2), 8656–8667. doi: https://doi.org/10.1016/j.ifacol.2020.12.315.

Singhose, W. (2009). Command shaping for flexible systems: A review of the first 50 years. *International Journal of Precision Engineering and Manufacturing*, 10(4), 153–168.

Sobota, J., Goubej, M., Königsmarková, J., and Čech, M. (2019). Raspberry Pi-based HIL simulators for control education. *IFAC-PapersOnLine*, 52(9), 68–73. doi: https://doi.org/10.1016/j.ifacol.2019.08.126. 12th IFAC Symposium on Advances in Control Education.

Wang, Y., Gao, F., and Doyle, F.J. (2009). Survey on iterative learning control, repetitive control, and run-to-run control. *Journal of Process Control*, 19(10), 1589–1600. doi:https://doi.org/10.1016/j.jprocont.2009.09.006.

Yakub, M.F.M., Qadir, A., and Aminudin, B.A. (2012). Comparative study on control method for two-mass systems. *International Journal on Advanced Science, Engineering and Information Technology*, 2, 261–266.

Čech, M., Königsmarková, J., Goubej, M., Oomen, T., and Visioli, A. (2019). Essential challenges in motion control education. *IFAC-PapersOnLine*, 52, 200–205. doi:https://doi.org/10.1016/j.ifacol.2019.08.196.

Čech, M., Beltman, A.J., and Ozols, K. (2021). Pushing mechatronic applications to the limits via smart motion control. *Applied Sciences*, 11(18).